ELSEVIER

Journal of Membrane Science 193 (2001) 97–109

journal of MEMBRANE SCIENCE

www.elsevier.com/locate/memsci

# On the behavior of the electrostatic colloidal interaction in the membrane filtration of latex suspensions

Myung-Suk Chun [a,*], Gui-Yung Chung [b], Jae-Jin Kim [a]

[a] *Complex Fluids and Membranes Lab, Korea Institute of Science and Technology, P.O. Box 131, Cheongryang, Seoul 130-650, South Korea*
[b] *Department of Chemical Engineering, Hong-Ik University, Mapo-Ku, Seoul 121-791, South Korea*

Received 18 September 2000; received in revised form 20 April 2001; accepted 14 May 2001

**Abstract**

In order to investigate effects of the colloidal interaction in the membrane filtrations, the dead-end ultrafiltration of latex colloids was conducted with fully retentive membranes. Experimental results concerning the permeate flux during the filtration indicate that the void fraction of cake layer increased with the decrease of the ionic strength, due to the expanded Debye double layer thickness around the particles. The concentration dependence of the gradient diffusion coefficient of colloidal particles has been examined as a function of solution ionic strength. The NVT Monte Carlo simulation was applied on the bulk suspension so as to determine the thermodynamic coefficient, and the hydrodynamic coefficient was evaluated from the previously developed relation for an ordered system. The long-range electrostatic interactions between the particles are determined by using a singularity method, which provides accurate solutions to the linearized electrostatic field. The predictions on the variation of concentration polarization layer have been presented, from which we found that both the permeate flux and the particle diffusion are related to determine the concentration distribution above the cake layer. 

*Keywords:* Electrostatic interaction; Permeate flux; Particle diffusion; Concentration polarization; Dead-end filtration; Colloidal suspensions

## 1. Introduction

Long-range colloidal interactions can have a dramatic effect on the membrane filtration of colloidal particles from liquid, where the colloids may be polymeric, biological, or inorganic. In the membrane filtrations such as an ultrafiltration and a microfiltration, the driving force for separation is a transmembrane pressure drop [1,2]. In the fully retentive membranes, whether we employ a dead-end mode or a cross-flow mode, the retained solute particles at the membrane surface build up with time as a cake layer. The cake layer provides an additional increasing resistance to filtration, so that the permeate flux declines with time [3–5]. The retained solutes above the cake layer result in a concentration polarization (CP) layer with the spatially variable solute concentration.

There are numerous studies on the behavior of permeate flux decline in the membrane filtration of colloidal suspensions. Also, both the theory of the concentration polarization and the characteristics of the cake layer are considered to understand the membrane fouling mechanism. Note that the concentration profile above the cake layer is determined by the osmotic pressure and the permeate flux across the membrane [6]. However, systematic studies that examine the coupled effects of hydrodynamic and physicochemical conditions on the permeate flux as well as on the CP layer are scarce.

* Corresponding author. Fax: +82-2-958-5308.
*E-mail address:* mschum@kist.re.kr (M.-S. Chun).

0376-7388/01/$ – see front matter 
PII: S0376-7388(01)00501-4

**Nomenclature**

| | |
|---|---|
| $a$ | particle radius (m) |
| $A_H$ | Hamaker constant (J) |
| $A_2$, $A_3$ | osmotic virial coefficients |
| $C$ | particle volume fraction |
| $C_b$ | particle volume fraction in the bulk |
| $C_c$ | particle volume fraction in the cake layer |
| $D$ | gradient diffusion coefficient ($m^2/s$) |
| $D_0$ | dilute limit diffusion coefficient ($m^2/s$) |
| $e$ | elementary electrostatic charge (C) |
| $\boldsymbol{e}$ | unit vector |
| $E$ | interaction energy (J) |
| $F$ | electrostatic force (N) |
| $g$ | radial distribution function |
| $\boldsymbol{I}$ | identity tensor |
| $k$ | Boltzmann constant (J/K) |
| $K$ | hydrodynamic coefficient |
| $\boldsymbol{n}$ | unit normal vector pointing into solvent |
| $N_{Fc}$ | critical filtration number |
| $\Delta p$ | transmembrane pressure drop ($N/m^2$) |
| $\Delta p_p$ | pressure drop on the polarization layer ($N/m^2$) |
| $R_c$ | cake resistance ($m^{-1}$) |
| $\hat{R}_c$ | specific cake resistance ($m^{-2}$) |
| $R_m$ | membrane resistance ($m^{-1}$) |
| $s$ | center-to-center separation distance (m) |
| $S$ | thermodynamic coefficient |
| $S_A$ | surface area ($m^2$) |
| $t$ | filtration time (s) |
| $T$ | absolute temperature (K) |
| $\boldsymbol{T}$ | Maxwell stress tensor defined in Eq. (19) ($N/m^2$) |
| $v$ | permeate flux (m/s) |
| $V$ | streaming potential (V) |
| $x$ | Cartesian coordinate |
| $y$ | distance from the cake layer (m) |

*Greek letters*

| | |
|---|---|
| $\beta$ | compressibility factor |
| $\delta_c$ | cake layer thickness (m) |
| $\varepsilon$ | dielectric constant (C/V m) |
| $\zeta$ | zeta potential (V) |
| $\eta$ | viscosity of the solution (kg/m s) |
| $\kappa$ | inverse Debye length ($m^{-1}$) |
| $\lambda_0$ | bulk solution conductivity (S/m) |
| $\Xi$ | a factor defined in Eq. (25) ($s^{-1}$) |
| $\Pi$ | osmotic pressure ($N/m^2$) |
| $\sigma$ | dimensionless surface charge density defined in Eq. (15) |
| $\psi$ | electrostatic potential (V) |
| $\psi_{s,p}$ | dimensionless surface potential of solute particle |
| $\psi_{s,w}$ | dimensionless surface potential of wall |

*Subscripts*

| | |
|---|---|
| $r$, $\theta$, $\varphi$ | elements of spherical coordinate |

Properties of the bulk suspension of charged colloids are closely related to the development of CP layer. In this respect, the gradient diffusion coefficient is a key parameter in a large number of processes involving colloidal particles, such as a membrane filtration [7]. However, the calculation of the gradient diffusion coefficient is not a succinct problem because the calculation of multiparticle interactions is so complicated. Although the colloidal interactions originate from the various forces, the two most important are the electrostatic repulsion and the attractive dispersion forces [8]. Many attempts have been made at examining the osmotic pressure for colloidal suspensions with multiparticle interactions. Among them, it is noted that the osmotic pressure can be properly estimated by employing a cell model method [9]. By the solution of the non-linear Poisson–Boltzmann (P–B) equation within a cell, it is possible to calculate the repulsive force between two particles taking into account the effect of the neighboring particles.

The electrostatic interaction energies between particles are significantly changed by the variation of solution ionic strength, relating the Debye length. In the present study, we applied the singularity method previously proposed as a useful scheme for multisphere systems [10] with the linearized P–B equation. If the dielectric constant is assumed to be small relative to that of the surrounding liquid, then the electrostatic potential in the liquid can be represented as a sum of contributions from point charges located inside the particles. These point charges are expressed by the fundamental singular solution to the linearized P–B equation. The strengths of the singularities are chosen so as to provide the best possible agreement with the prescribed boundary conditions.

We consider an analytical model for the prediction of the concentration profile above cake layer during the dead-end membrane filtration of colloids, and changes of the permeate flux of polystyrene latex is observed with the filtration time. Based on the estimations of the cake porosity and the cake compressibility, effects of the expanded double layer around particle surfaces on the filtration properties are examined. In order to estimate the gradient diffusion coefficient, the analytical expressions in combination with the Monte Carlo method is considered as a predictive method for the thermodynamic coefficient. We determine the interaction energy profile between pairs of particles at the conditions of latex suspension used in this study. The hydrodynamic coefficient can be predicted from the relation for an ordered suspension. The concentration dependence of the gradient diffusion coefficient of colloidal particles is investigated as a function of the solution ionic strength.

## 2. Basic considerations on the dead-end filtration

Unlike the cross-flow filtration, all particles brought to the membrane surface by the permeate flow can deposit on the surface during the dead-end filtration using a fully retentive membrane which maintains a complete solute rejection. Here, the distribution of the particle concentration above the cake layer is described with a one-dimensional convective diffusion equation. The flux decline observed in colloidal particles has been attributed to many of the complicated physicochemical phenomena.

In the dead-end filtration shown in Fig. 1, suspended particles form a CP layer above the cake layer built by particle depositions on the membrane surface. At a steady-state, the differential material balance describing the accumulation of colloidal particles along the *y* direction in the CP layer can be considered. At any axial position of the filtration channel, it takes the

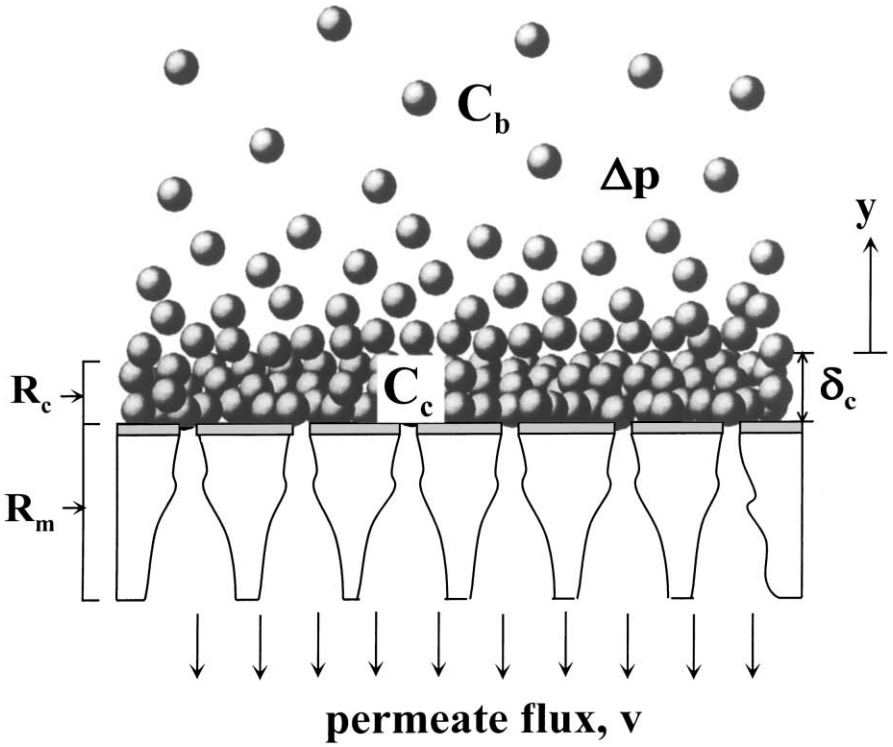


Fig. 1. Schemetic diagram of dead-end filtration of colloidal suspension.

following form:

$$v\frac{\partial C}{\partial y} + D\frac{\partial^2 C}{\partial y^2} = 0 \tag{1}$$

where $C$ is the particle concentration, $v$ the permeate flux in the transverse (i.e. $y$) direction, and $D$ the particle diffusion coefficient. The boundary conditions on the membrane or the cake surface and into the bulk suspension are described by

$$C = C_c \text{ at } y = 0 \tag{2}$$

$$C = C_b \text{ at } y \to \infty \tag{3}$$

where $C_b$ and $C_c$ are the particle concentrations in the bulk suspension and in the cake layer, respectively. The solution of Eq. (1) subject to the above boundary conditions interestingly results in the concentration distribution in the CP layer

$$C = \exp\left(-\frac{v}{D}y\right)(C_c - C_b) + C_b \tag{4}$$

Then, Eq. (4) means that the concentration distribution of particles in the CP layer is determined by the permeate flux ($v$) as well as the particle diffusion coefficient ($D$).

The permeate flux $v$ incorporating with the boundary layer model is described by the Darcy's law for the overall hydraulic resistance in terms of membrane, cake, and polarization resistance in series. With employing the effective pressure drop on both the membrane and the cake layer, the general filtration equation can be expressed [4] as follows:

$$v = \frac{\Delta p - \Delta p_p}{\eta(R_m + R_c)} \tag{5}$$

where $\Delta p$ is the transmembrane pressure drop imposed across the cake and the membrane, $\Delta p_p$ the pressure drop on the CP layer, $\eta$ the solution viscosity, $R_m$ the membrane resistance, and $R_c$ the cake resistance. When a cake layer is present on the membrane surface, the $\Delta p_p$ is maintained at a critical value. This critical pressure is, independent of the applied pressure and the permeate flux, solely determined by the thermodynamic properties of the suspensions. For a monodispersion, the critical pressure is determined by

$$\Delta p_p = \frac{3kT}{4\pi a^3}N_{Fc} \tag{6}$$

where $k$ is the Boltzmann constant, $T$ the absolute temperature, $a$ the particle radius, and $N_{Fc}$ the critical filtration number, which is 15 for uniform rigid spherical particles at a cake concentration of 0.64 [6]. The particle accumulation in the cake layer provides an additional resistance to the permeate flow, from which this resistance causes the permeate flux to decline. Note that the cake resistance is a product of the specific cake resistance and the cake thickness defined as follows:

$$R_c = \hat{R}_c\delta_c \tag{7}$$

When the particle diameter is larger than the membrane pore diameter like the case of fully retentive, the cake resistance is likely to change alone.

## 3. Particle diffusion and long-range interaction

### 3.1. Diffusion in the colloidal suspensions

As provided in Eq. (4), the estimation of diffusion coefficient is necessary to determine the concentration distribution. The diffusion coefficient of a particle in the bulk can be obtained from the well-known Stokes–Einstein equation as the following expression [7]:

$$D_0 = \frac{kT}{6\pi\eta a} \tag{8}$$

At finite concentrations, both colloidal interactions and hydrodynamic interactions mediated by the fluid modify the dilute limit value. The generalized Stokes–Einstein equation valid over the entire range of particle concentrations can be used to evaluate the gradient diffusion coefficient [7,8] as follows:

$$D(C) \equiv D_0\frac{K(C)}{S(C)} = D_0K(C)\left[\frac{\partial\Pi(C)}{\partial C}\frac{4\pi a^3}{3kT}\right] \tag{9}$$

where $S(C)$ is the thermodynamic coefficient determined from the osmotic pressure $\Pi(C)$, and $K(C)$ the hydrodynamic coefficient. The osmotic pressure is expressed in the form of virial equation as follows:

$$\Pi(C) = \frac{3kT}{4\pi a^3}C(1 + A_2C + A_3C^2 + \cdots) \tag{10}$$

where $A_2$ and $A_3$ are osmotic virial coefficients. Note that the coefficient $S(C)$ coincides with the structure

factor of the suspension at the zero scattering vector. It is possible to derive the analytical solution in power series of the particle concentration as:

$$S(C) = 1 - 2A_2C + (2A_2^2 - 3A_3)C^2 + O(C^3) \quad (11)$$

Here, $A_2$ is represented by

$$A_2 = \frac{3}{2a^3}\int_0^\infty [1 - g(s)]s^2\,\mathrm{d}s = \frac{3}{2a^3}\int_0^\infty \left[1 - \exp\left(-\frac{E(s)}{kT}\right)\right]s^2\,\mathrm{d}s \quad (12)$$

where $s$ is the center-to-center separation distance, $g(s)$ the radial distribution function, and $E(s)$ the pairwise interaction energy. As mentioned before, $E$ equals to a sum of both repulsive potential and attractive potential. The radial distribution function for a concentrated suspension can be determined by integral equations, perturbation methods, and Monte Carlo simulations. Monte Carlo simulations are employed in this study, since they enable the prediction of the charged suspension over the full range of particle concentrations.

The hydrodynamic coefficient $K(C)$ accounts for the fact that the drag force in concentrated suspensions exerted on a single particle deviates from the Stokes law due to the presence of neighboring particles. In principle, this coefficient expressed as the ratio of the sedimentation velocity of a single particle to that of mean velocity of a suspended particle describes the sedimentation velocity of an assemblage of spheres. We calculated $K(C)$ using Happel and Brenner equation for ordered suspensions, given as follows [11]:

$$K(C) = \frac{1 - (3/2)C^{1/3} + (3/2)C^{5/3} - C^2}{1 + (2/3)C^{5/3}} \quad (13)$$

It is possible to estimate an effective hard sphere radius from the perturbation theory [12], and the particle concentration in Eq. (13) is then corrected as a function of the interaction energy between pairs of particles. However, it can be reasonably assumed that the effective hard sphere radius is nearly equal to the hydrodynamic radius, which corresponds to an addition of the hard sphere radius $a$ and the thickness of the inner region of double layer. As a result, the correction effect is almost negligible.

### 3.2. Electrostatic interaction energy

When two colloidal particles are charged, electrostatic interactions contribute to the energy $E$ of Eq. (12). The classic approach has been to use the Derjaguin approximation when the Debye length is small compared to the curvature of the surfaces, and to use the linear superposition approximation when the separation distance is larger than the Debye length. However, it has been found that the Derjaguin approximation is inaccurate when the Debye length is comparable to the sphere size. At small separations, for constant surface potentials the linear superposition approximation tends to overpredict the force, whereas for constant charge conditions the predicted force is too low. The singularity method applied in the present study can be evidently overcome the restrictions described above. We introduce the method by considering a problem of $N$ identical, charged spheres interaction with the electrostatic potential governed by a linearized P–B equation

$$\nabla^2\psi - (\kappa a)^2\psi = 0 \quad (14)$$

where the electrostatic potential $\psi$ is normalized by a characteristic surface potential, and the inverse Debye length $\kappa$ is made dimensionless by the particle radius $a$. Two kinds of boundary conditions, which correspond to the constant charge and the constant potential conditions, can be commonly used in obtaining solutions to Eq. (14). Here, we consider the particle and pore surfaces $S_A$ have a constant surface-charge density $\sigma$, leading to the constant charge boundary condition

$$\boldsymbol{n} \cdot \nabla\psi = \sigma \text{ on } S_A \quad (15)$$

where $\boldsymbol{n}$ denotes a unit normal vector. Except for only surface separations so small as to be rendered highly improbable, the linearized P–B equation with constant charge boundary conditions provides good accuracy. From the singular solution to Eq. (14) for a point charge at the origin, each of the dimensionless surface charge densities of the pore wall and the particle are expressed as follows:

$$\sigma_w = \psi_{s,w}(\kappa a), \quad \text{for wall} \quad (16)$$

$$\sigma_p = \psi_{p,w}(\kappa a + 1), \quad \text{for particle} \quad (17)$$

Both the pore wall and the particles, when they are isolated and not interacting with each other, have surface potentials equal to $kT/e = 25.69\,\text{mV}$, where $e$ is the elementary electrostatic charge.

The force on a charged sphere interacting with other charged spheres is calculated by accounting for the spherical coordinate with each components of unit vector $\boldsymbol{e}_r$, $\boldsymbol{e}_\theta$, $\boldsymbol{e}_\varphi$. A pointwise distribution is developed as the solution, and the strength of each point singularity is determined by satisfying the boundary conditions, from which an accurate solution of P–B equation is provided. The force vector $\boldsymbol{F}$ is calculated from the surface integration of normal component of Maxwell stress tensor $\boldsymbol{T}$, as follows:

$$\boldsymbol{F} \equiv \int_{S_\text{A}} \boldsymbol{T} \cdot \boldsymbol{n}\, \mathrm{d}S_\text{A} \tag{18}$$

The Maxwell stress tensor is given by

$$\boldsymbol{T} = \left(\Pi + \varepsilon \frac{\boldsymbol{E}\cdot\boldsymbol{E}}{2}\right)\boldsymbol{I} - \varepsilon \boldsymbol{E}\cdot\boldsymbol{E} \tag{19}$$

where $\varepsilon$ is a dielectric constant, $\boldsymbol{I}$ is the identity tensor, and $\boldsymbol{E}(= -\nabla\psi)$ denotes the electric field vector. The electrostatic potential is related to the osmotic pressure $\Pi(= \varepsilon\kappa^2\psi^2/2)$. Then, the electrostatic interaction energy profile between pairs of particles with separation distance can be obtained by integrating the force acting on the sphere as follows:

$$\begin{aligned} E_\text{EL}(s-2a) &= \int_{-\infty}^{s-2a} F_x\, \mathrm{d}x \\ &= \int_{-\infty}^{s-2a} \left[\boldsymbol{e}_x \cdot \int_{S_\text{A}} \boldsymbol{T}\cdot\boldsymbol{n}\, \mathrm{d}S_\text{A}\right] \mathrm{d}x \\ &= \int_{S_\text{A}} [\cos\theta\, \boldsymbol{e}_r \cdot \boldsymbol{T}\cdot\boldsymbol{e}_r \\ &\quad -\sin\theta\, \boldsymbol{e}_\theta \cdot \boldsymbol{T}\cdot\boldsymbol{e}_r]\, \mathrm{d}S_\text{A} \end{aligned} \tag{20}$$

where $\mathrm{d}S_A = r^2 \sin\theta\, \mathrm{d}\theta\, \mathrm{d}\varphi$. More detailed description on the computational procedure for Eq. (20) can be found in the previously reported paper [10].

### 3.3. Attractive van der Waals interaction energy

The van der Waals dispersion forces between the atoms in two approaching colloids are additive and result in an attractive force which acts over a relatively long range. Based on a pairwise summation method, the interaction energy between two identical colloids of radius $a$ can be obtained by

$$E_\text{VW} = -\frac{A_\text{H}}{6}\left[\frac{2a^2}{s^2-4a^2} + \frac{2a^2}{s^2} + \ln\left(1-\frac{4a^2}{s^2}\right)\right] \tag{21}$$

where $A_\text{H}$ denotes the Hamaker constant.

## 4. Experiments

### 4.1. Membrane and colloidal particle

The poly(acrylonitrile-co-vinyl chloride) XM50 flat membrane purchased from Millipore (Beverly, MA) was used, with a molecular weight cut-off of $5 \times 10^4$ Da. The morphology of a cross-section and the skin layer thickness were observed with a field emission scanning electron micrograph (FE-SEM, Hitachi Ltd., S-4200). Both the mean pore diameter and the surface pore density were estimated as 5.5 nm and $1.1 \times 10^{11}/\text{cm}^2$, in respect. The XM50 membrane has an asymmetric pore geometry, in which the pore depth can be determined as 16.7 nm calculated from the water flux (i.e. $0.84\,\text{cm}^3/\text{cm}^2\,\text{min atm}$) using Poiseuille equation.

As a model colloid, monodisperse polystyrene latex (LB-1, Sigma Chemical Co., MO) with a mean diameter of 0.1 μm was used. All experiments were carried out with latex suspensions of 200 ppm, and the ionic strengths of the suspension were controlled by the addition of KCl electrolyte. The solutions were prepared by using doubly distilled and deionized water. The rejection for latex suspension was determined by a comparison of latex concentrations in the feed and in the permeate using an UV detector (Rainin, Model Dynamax UV-1, CA). Its value results in above 98%, meaning a fully retentive behavior of XM50 membrane.

### 4.2. Permeate flux and zeta potential measurements

Details of ultrafiltration system and procedures have been described elsewhere [1–3]. The dead-end ultrafiltration experiments were carried out in a 50 ml Amicon batch cell (Model 8050, MA) removing a

stirring bar, in which the total area of membrane surface was $\pi(2.07)^2\,\mathrm{cm}^2$. The reservoir was connected to the batch cell for the filtration with long time and the transmembrane pressure drop was set precisely by nitrogen pressurization. The amount of permeate collected in time was determined by continuously weighing on an electronic balance (Mettler, Model PG 502, Switzerland), and then it was registered simultaneously by data acquisition program (BalanceLink Version 2.20, Mettler-Toledo AG).

The membrane zeta potential, $\zeta$, related to the electrokinetic properties of the membrane, is estimated using the Helmholtz–Smoluchouski equation [13]

$$\frac{\Delta V}{\Delta p} = \frac{\varepsilon\zeta}{\eta\lambda_0} \tag{22}$$

where $V$ is the streaming potential of the membrane, and $\lambda_0$ the solution conductivity. The membrane zeta potential was determined from streaming potential measurements, by using the equipment properly developed in our laboratory. The streaming potential difference was measured with variations of the transmembrane pressure drop, from which the linear relationship between $\Delta V$ and $\Delta p$ was obtained. The zeta potential of latex was determined using a Zeta-Plus (Brookhaven Instrument Co., NY). The value of the zeta potential was calculated from the mobility values based on a Doppler principle together with the particle velocity obtained by Smoluchouski formula. Fig. 2 exhibits that the XM membrane is negatively charged, but it is considered to be weakly charged due to a lower magnitude of zeta potential. It appears the magnitude of the negative zeta potential increases with increasing of ionic strength. The latex surfaces are negatively charged likewise the membrane pore, where its magnitude of zeta potential was greater than that of the membrane pore. Compared to the membrane zeta potential, the variance range on the zeta potential of latex is somewhat large.

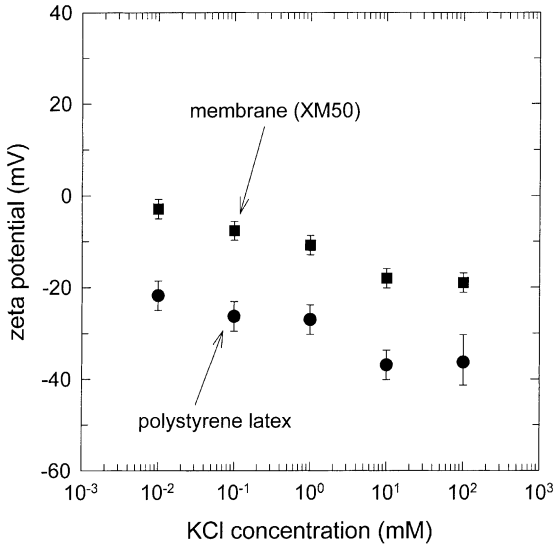


Fig. 2. The plots of zeta potential vs. solution ionic strength for XM50 membrane and polystyrene latex, where the solution has a condition of pH 6.0 and the latex concentration is 200 ppm.

## 5. Results and discussions

### 5.1. Permeate flux and cake layer

Fig. 3 displays the variations of permeate flux with the filtration time at different transmembrane pressure drops. As the pressure drop increases the permeate flux increases, in which the corresponding flux decline is also considerable. In Fig. 4, the variations of permeate flux with different ionic strengths demonstrate a lesser degree of effects compared to Fig. 3. It is obvious that,

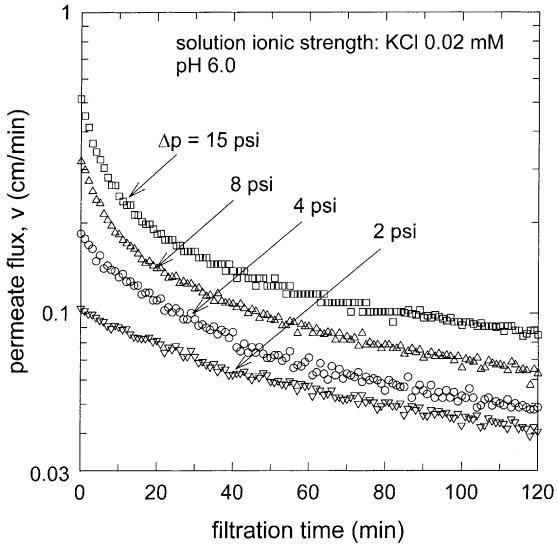


Fig. 3. The variation of permeate flux with filtration time at different transmembrane pressure drops, where the latex concentration is 200 ppm.

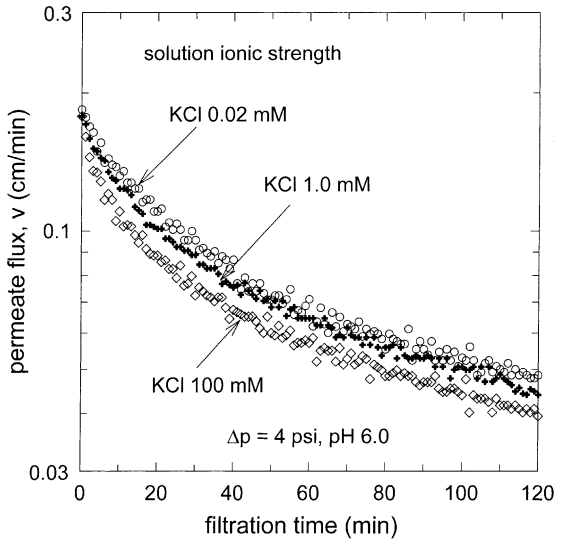


Fig. 4. The variation of permeate flux with filtration time at different ionic strengths, where the latex concentration is 200 ppm.

however, the permeate flux increases with decreasing of the ionic strength. This behavior allows us to examine the long-range electrostatic interaction between pairs of latex particles. The Debye length $\kappa^{-1}$ (nm) is given by [solution ionic strength $(M)$]$^{-1/2}$/3.278 for aqueous solutions of monovalent electrolytes at 25°C. The Debye lengths are estimated as 68.21, 9.65, and 0.96 nm, corresponding to the ionic concentrations of 0.02, 1.0, and 100 mM of KCl electrolyte. The increased electrostatic (Debye) double layer around particle surfaces with decreasing of the ionic strength leads to a particle location separated rather sparsely. As a consequence, the void fraction in the cake layer increases with decreasing of the ionic strength, and then the permeate flux increases accordingly.

From the mass balance of particles during the dead-end filtration, a first-order ordinary differential equation for cake layer thickness $\delta_c(t)$ is generated [4,5]. Performing the integration in terms of $d\delta_c(t)/dt$ with the initial condition yields the permeate flux and the cake thickness

$$v(t) = \frac{\Delta p - \Delta p_p}{\eta R_m}(1 + \Xi)^{-1/2} \tag{23}$$

$$\delta_c(t) = \frac{R_m}{\hat{R}_c}[(1 + \Xi)^{1/2} - 1] \tag{24}$$

where

$$\Xi = \frac{2\hat{R}_c C_b(\Delta p - \Delta p_p)}{(C_c - C_b)\eta R_m^2} \tag{25}$$

The membrane resistance $R_m$ is determined from the water flux, depending on the mean pore radius and the surface porosity. The specific cake resistance is estimated with the Carman–Kozeny equation [4] as follows:

$$\hat{R}_c = \frac{45}{a^2}\frac{C_c^2}{(1 - C_c)^3} \tag{26}$$

After fitting the variations of permeate flux with Eq. (23), the factor $\Xi$ can be determined, and then we favorably obtain the particle concentration in the cake as well as the cake layer thickness. The variations of cake layer thickness with the filtration time at different transmembrane pressure drops are shown in Fig. 5. The trend of growing a cake layer can be understood from Eq. (24), which means a $t^{1/2}$ dependence of the cake layer thickness. The cake layer thickness increases as the pressure drop increases, owing to a fully retentive characteristic of XM50 membrane for latex particles. The variations of cake layer thickness with the filtration time at different solution ionic strengths are shown in Fig. 6. At a given pressure drop,

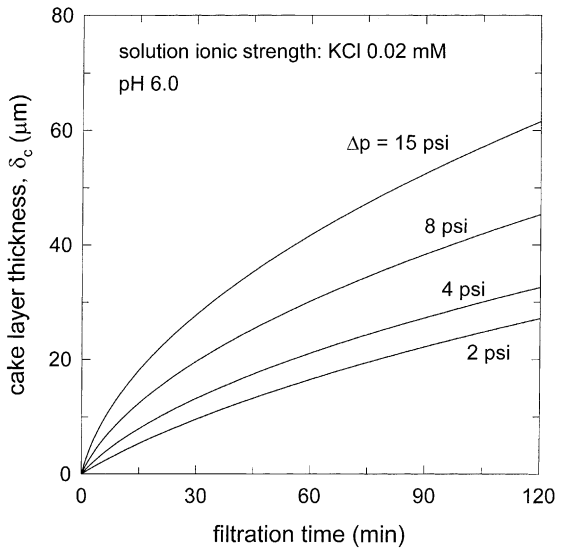


Fig. 5. The variation of cake layer thickness with filtration time at different transmembrane pressure drops, where the latex concentration is 200 ppm.

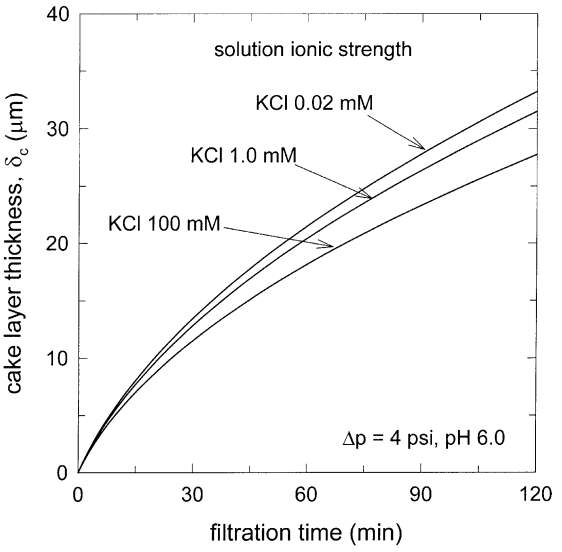


Fig. 6. The variation of cake layer thickness with filtration time at different ionic strengths, where the latex concentration is 200 ppm.

the cake layer thickness increases with decreasing of ionic strength. As described above, the electrostatic double layers existing around particle surfaces are expanded with decreasing solution ionic strength, which provides the development of loosely packed cake layer during the membrane filtration. As a result, the growth of cake layer increases with decreasing ionic strength.

The quantitative analysis provided in Table 1 shows that both the particle concentration in the cake and the specific cake resistance increase with increasing of either transmembrane pressure drop or ionic strength. The dependence of the specific cake resistance on the transmembrane pressure drop can be expressed by the power law function, $\hat{R}_c/C_c \approx \Delta p^{\beta}$ [2]. Interestingly, the compressibility factor $\beta$ varies from zero for completely incompressible materials to near unity for highly compressible materials. The value of $\beta$ of latex particle is almost zero at a sufficiently higher ionic strength, but the value of $\beta$ increases with decreasing of the ionic strength. It should be noted that the higher value of $\beta$ represents a soft compressible behavior of a highly charged latex due to an increased double layer.

### 5.2. Particle diffusion

Plotted in Fig. 7 is the particle–particle interaction energy at different $\kappa a$, in which we have taken the average value of surface potential of latex particles as 25.69 mV based on the results of Fig. 2. The Hamaker constant was chosen to be $5 \times 10^{-21}$ J for the polystyrene latex in an aqueous medium [14]. As the solution ionic strength increases, the repulsion energy decreases but the attraction energy increases. Note that a minimum occurs at a closer distance for the solution ionic strength of 100 mM, due to dominant attraction energy.

The Metropolis Monte Carlo simulations sampled a canonical ensemble for which the number of particles, temperature, and volume are constant (i.e. NVT). The canonical ensemble is represented with the probability

Table 1
The estimation of particle concentration in the cake layer, specific cake resistance, and compressibility factor

| KCl concentration (mM) | $\Delta p$ (psi) | $C_c$ | $\hat{R}_c$ ($10^{13}$ cm$^{-2}$) | Compressibility factor, $\beta$ |
|---|---|---|---|---|
| 0.02 | 2.0 | 0.516 | 0.748 | 0.249 |
| | 4.0 | 0.558 | 0.819 | |
| | 8.0 | 0.569 | 0.965 | |
| | 15.0 | 0.576 | 1.057 | |
| 1.0 | 2.0 | 0.519 | 0.767 | 0.191 |
| | 4.0 | 0.563 | 0.883 | |
| | 8.0 | 0.577 | 1.080 | |
| | 15.0 | 0.582 | 1.169 | |
| 100 | 2.0 | 0.526 | 0.819 | 0.095 |
| | 4.0 | 0.579 | 1.117 | |
| | 8.0 | 0.589 | 1.280 | |
| | 15.0 | 0.591 | 1.291 | |

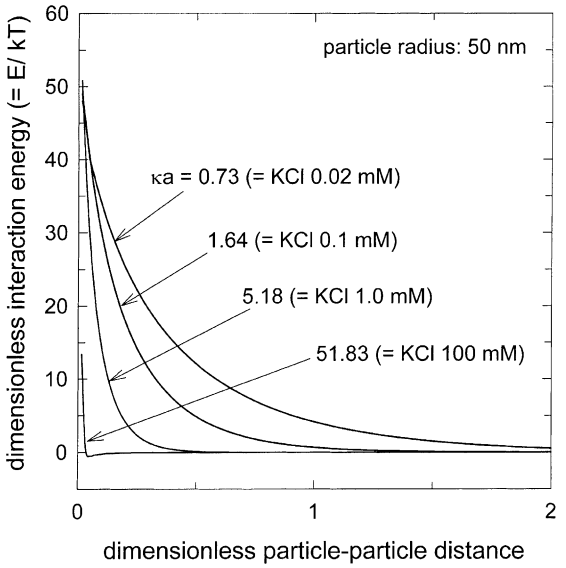


Fig. 7. Dimensionless energy profiles for particle–particle interactions for several inverse Debye lengths with constant surface-charge boundary conditions and pH 6.0.

of observing the $i$th state, such that

$$p_i = \frac{\exp[-E_i(N, V)/kT]}{\sum_i \exp[-E_i(N, V)/kT]}$$

where the denominator corresponds to the partition function [15,16]. The basic procedure for the NVT Monte Carlo is to displace a particle randomly for the periodic unit cell constructed with Cartesian coordinates. In the NVT process, the probability governing the particle displacement is justified as $\min[1, \exp(-\Delta E/kT)]$, where $\Delta E = E_{\text{trial}} - E_i$. If the random number is less than this probability, the respective moves are accepted, otherwise the moves are rejected. During the simulations, the total energies after the particle displacements are evaluated by using a pair-wise additive principle with respect to particle–particle interactions. Interpolating with polynomials is adopted so as to determine instantaneously the interaction energy at arbitrary particle–particle separation distances [17]. In the present study, particles with a total number of 500–800 are introduced in a simulation box. Discarding non-equilibrium configurations and production configurations are taken to about $2 \times 10^4$ and $4 \times 10^4$, in respect. The test for overlapping in random movements of particles is carried out with a square well mode.

The radial distribution function obtained by Monte Carlo is changed with the variations of particle concentration. When the particle concentration is zero, the coefficient $A_2$ has a maximum value corresponding the dilute limit $A_2$. The values of dilute limit $A_2$ result in 4.05, 1.9, 0.7, and 0.23 for the solution ionic strength of 0.02, 0.1, 1.0, and 100 mM, respectively. We can find the dependence of particle concentration on the value of $A_2$ at different solution ionic strengths, in which the value of $A_2$ decreases with increasing of the particle concentration. Once the values of $A_2$ are known, both the thermodynamic coefficient and the osmotic pressure can be computed as a function of the particle concentration. Fig. 8 shows the calculated values of the thermodynamic coefficient $S$ at different ionic strengths, where the dotted lines indicate the hypothetical results obtained by using the dilute limit $A_2$. At a higher value of KCl concentration, such as 100 mM, the value of $S$ decreases almost linearly with increasing of the particle concentration. At a lower KCl concentration, the decrease of the value of $S$ with increasing of the particle concentration is significant.

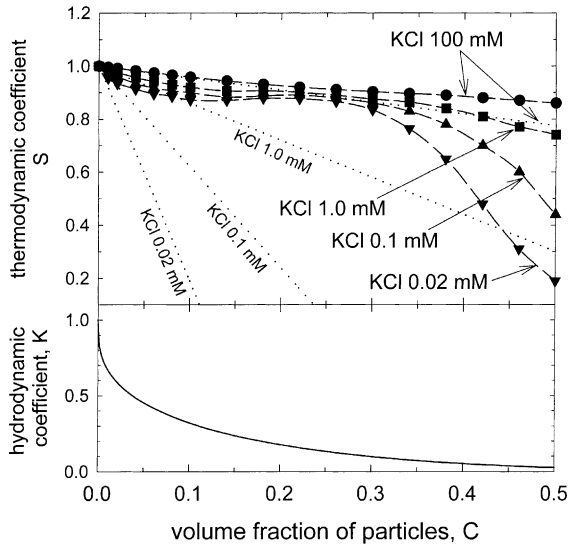


Fig. 8. The plots of thermodynamic coefficient $S$ as well as hydrodynamic coefficient $K$ vs. particle concentration with different solution ionic strengths at pH 6.0. Dotted lines correspond to the predictions obtained using $A_2$ coefficients for dilute limit case.

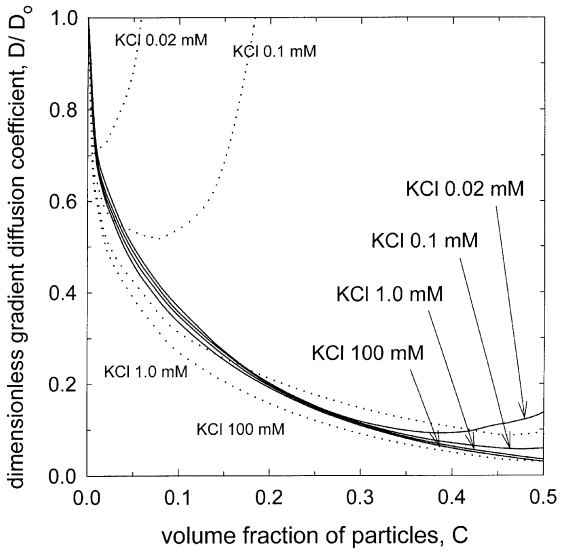


Fig. 9. The plots of dimensionless gradient diffusion coefficient vs. particle concentration with different solution ionic strengths at pH 6.0. Dotted curves correspond to the predictions obtained using $A_2$ coefficients for dilute limit case.

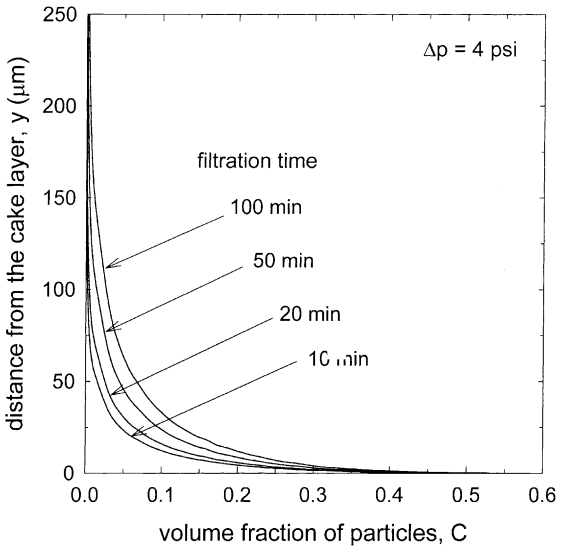


Fig. 10. The variation of concentration profile of latex particle at filtration time of 10, 20, 50, and 100 min. Experimental conditions are transmembrane pressure drop of 4 psi, KCl 1.0 mM, and pH 6.0.

Here, the decreasing tendency of the value of $S$ for the particle concentration of above about 0.25 should be noted. Whereas the thermodynamic coefficient $S$ shows a clear dependence on the solution ionic strength, the hydrodynamic coefficient $K$ becomes entirely the limit value of a hard sphere regardless of the KCl concentration. As demonstrated in Fig. 8, the hydrodynamic coefficient $K$ experiences a decay as the particle concentration increases, and the value of $K$ almost becomes zero for the particle concentration of above 0.6.

In Fig. 9, the calculated values of the gradient diffusion coefficient are provided for the particle concentrations ranging from a dilute limit to a high value. The variation of diffusion coefficient with the particle concentration exhibits an initial decrease. The dependence of the solution ionic strength on the diffusion coefficient is weak for the particle concentrations up to about 0.3. Basically, this is due to the fact that the surface potential of a latex particle used in this study is low such as the dimensionless order of unity. Further, the contribution of an attractive interaction results in the lower dependence of the thermodynamic coefficient $S$ on the particle concentration. Above the particle concentration of 0.3, however, the diffusion coefficient shows a rise up behavior for the solution ionic strength of 0.02 and 0.1 mM. The diffuison coefficient increases with the decrease of the solution ionic strength, which implies an enhancement in the particle diffusion due to an increase of the electrostatic repulsion.

### 5.3. Concentration profile above the cake layer

The distribution of latex concentration above the cake layer is determined by Eq. (4), with the corresponding permeate flux observed by experiments and the diffusion coefficient obtained theoretically. Fig. 10 shows the behavior of CP layer with the progress of filtration time at the transmembrane pressure drop $\Delta p$ of 4 psi. The particle concentration decreases from $C_c$ at the region of cake layer to $C_b$ (200 ppm) at the region of bulk suspension. This figure indicates that the thickness of CP layer is up to about 200 μm. As the filtration proceeds, the local distribution of particle concentration increases. The growth of the CP layer is incorporated to the development of the cake layer above the membrane surface. At a given filtration time 50 min, the thickness of the CP layer decreases with

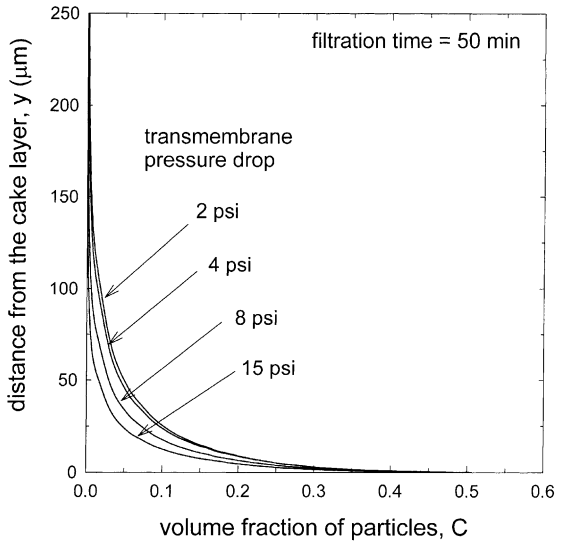


Fig. 11. The variation of concentration profile of latex particle at transmembrane pressure drop of 2, 4, 8, and 15 psi. Experimental conditions are filtration time of 50 min, KCl 1.0 mM, and pH 6.0.

the increase of the transmembrane pressure drop, as provided in Fig. 11.

The variation of concentration profile due to the different solution ionic strength is not seen in the CP layer. It should be pointed out that the electrostatic interaction in the bulk suspension is weak due to a low surface potential of latex particle used in this study, as given in Fig. 2. If the particle suspensions with a high surface potential were used, the evident dependence of the electrostatic interaction on the concentration profile could be expected.

## 6. Conclusions

A fundamental attempt to examine the membrane filtration of colloidal suspensions requires adequate knowledge of the influence of colloidal interactions. Up to now, many researches in terms of the behavior of electrostatic interaction and the electrokinetic properties have been carried out.

It is obvious that the long-range electrostatic interaction affects the permeate flux, the cake formation, and the particle diffusion during the membrane filtration. Note that the permeate flux, influenced by both the transmembrane pressure drop and the solution conditions, increases with the increase of the electrostatic interaction, which is readily related to the porosity of particles within the cake layer. As the solution ionic strength decreases, the estimated specific cake resistance decreases, whereas the cake compressibility increases. These phenomena can be understood by the fact that the expanded double layer around particle surfaces provides an increased repulsion and, as a result, the possible formation of a loosely packed cake layer.

We know that both the permeate flux and the particle diffusion control the concentration distribution of particles above the cake layer during the dead-end filtration. Predictions of the gradient diffusion coefficient depends on the accurate determinations of both the thermodynamic coefficient and the hydrodynamic coefficient. The characteristics of the membrane and the polystyrene latex charged weakly were identified from the measurements of zeta potential. Our computations on the interaction energy profile based on the singularity method provide the accurate results whether the values of dimensionless Debye length (i.e. $\kappa a$) are large or small. The effect of solution ionic strength on the particle diffusion depends on the particle concentration. The effect of the electrostatic interaction on the particle diffusion is evident for the particle concentration of above about 0.3.

## Acknowledgements

This work was partially supported by the environmental research fund (Green Korea 21C) of KIST provided to M.-S. Chun. The authors acknowledge the Chemical Engineering Department at the Korea Advanced Institute of Science and Technology (KAIST) for the use of electrokinetic facilities (Zeta-Plus) for the measurement of the zeta potential of latex particles.

## References

[1] L.J. Zeman, A.L. Zydney, Microfiltration and Ultrafiltration: Principles and Applications, Marcel Dekker, New York, 1996.
[2] G. Belfort, R.H. Davis, A.L. Zydney, The behavior of suspensions and macromolecular solutions in cross-flow microfiltration, J. Membr. Sci. 96 (1994) 1–58.
[3] G.B. van den Berg, C.A. Smolders, The boundary-layer resistance model for unstirred ultrafiltration: a new approach, J. Membr. Sci. 40 (1989) 149–172.

[4] L. Song, Flux decline in cross-flow microfiltration and ultrafiltration: mechanisms and modeling of membrane fouling, J. Membr. Sci. 139 (1998) 183–200.
[5] R.H. Davis, Modeling of fouling of cross-flow microfiltration membranes, Sep. Purif. Methods 21 (1992) 75–126.
[6] L. Song, M. Elimelech, Theory of concentration polarization in cross-flow filtration, J. Chem. Soc., Faraday Trans. 91 (1995) 3389–3398.
[7] W.R. Bowen, A. Mongruel, P.M. Williams, Prediction of the rate of cross-flow membrane ultrafiltration: a colloidal interaction approach, Chem. Eng. Sci. 51 (1996) 4321–4333.
[8] W.B. Russel, D.A. Saville, W.R. Schowalter, Colloidal Dispersions, Cambridge University Press, Cambridge, NY, 1989.
[9] W.R. Bowen, F. Jenner, Dynamic ultrafiltration model for charged colloidal dispersions: a Wigner–Seitz cell approach, Chem. Eng. Sci. 50 (1995) 1707–1736.
[10] R.J. Phillips, Calculation of multisphere linearized Poisson–Boltzmann interactions near cylindrical fibers and planar surfaces, J. Colloid Interface Sci. 175 (1995) 386–399.
[11] S. Hong, R.S. Faibish, M. Elimelech, Kinetics of permeate flux decline in cross-flow membrane filtration of colloidal suspensions, J. Colloid Interface Sci. 196 (1997) 267–277.
[12] J.A. Barker, D. Henderson, Perturbation theory and equation of state for fluids II: a successful theory of liquids, J. Chem. Phys. 47 (1967) 4714–4721.
[13] K.J. Kim, A.G. Fane, M. Nystrom, A. Pihlajamaki, W.R. Bowen, H. Mukhtar, Evaluation of electroosmosis and streaming potential for measurement of electric charges of polymeric membranes, J. Membr. Sci. 116 (1996) 149–159.
[14] C.A. Silebi, A.J. McHugh, An analysis of flow separation in hydrodynamic chromatography of polymer latexes, AIChE J. 24 (1978) 204–212.
[15] M.P. Allen, Introduction to Monte Carlo Simulation, in: M. Baus, L.F. Rull, J.-P. Ryckaert (Eds.), Observation, Prediction and Simulation of Phase Transitions in Complex Fluids, NATO ASI Series C, Vol. 460, Kluwer Academic Publisher, Dordrecht, 1994, pp. 339–356.
[16] R.J. Sadus, Molecular Simulation of Fluids: Theory, Alg- orithms and Object-Orientation, Elsevier, Amsterdam, 1999.
[17] M.-S. Chun, R.J. Phillips, Electrostatic partitioning in slit pores by Gibbs ensemble Monte Carlo simulation, AIChE J. 43 (1997) 1194–1203.